



## ORIGINAL ARTICLE

# In vitro and in vivo evaluation of hydrogel-based scaffold for bone tissue engineering application



Rongzhi Yang<sup>a</sup>, Rui Wang<sup>b</sup>, Saleheh Abbaspoor<sup>c</sup>, Mariappan Rajan<sup>d</sup>,  
Abduladheem Turki Jalil<sup>e</sup>, Marwan Mahmood Saleh<sup>f,g</sup>, Weizhuo Wang<sup>h,\*</sup>

<sup>a</sup> Department of Orthopedics, Luoyang Central Hospital Affiliated to Zhengzhou University, Luoyang, 471000, China

<sup>b</sup> Xi'an Jiaotong University, Xi'an, Shaanxi 710004, China

<sup>c</sup> Chemical Engineering Department, School of Engineering, Damghan University, Damghan, Iran

<sup>d</sup> Biomaterials in Medicinal Chemistry Laboratory, Department of Natural Products Chemistry, School of Chemistry, Madurai Kamaraj University, Madurai 625021, India

<sup>e</sup> Medical Laboratories Techniques Department, Al-Mustaqbal University College, Babylon, Hilla 51001, Iraq

<sup>f</sup> Department of Biophysics, College of Applied Sciences, University of Anbar, Iraq

<sup>g</sup> Medical Laboratory Technology Department, College of Medical Technology, The Islamic University, Najaf, Iraq

<sup>h</sup> Department of Orthopedics, The Second Affiliated Hospital, Xi'an Jiaotong University, Xi'an, Shaanxi 710004, China

Received 3 January 2023; accepted 8 March 2023

Available online 15 March 2023

## KEYWORDS

Bone regeneration;  
Nanofibrous carbon;  
Alginate;  
Carboxymethyl cellulose;  
Hydrogel

**Abstract** The main objective of the current assay was to fabricate a sophisticated and effective scaffold based on the nanofibrous structure in combination with the 3D structure of hydrogels for bone tissue engineering. In this scenario, we fabricated nanofibers using electrospinning and carbonized them. The processed nanofibers were added to the polymeric solution and cross-linked to embedded nanofibers into the 3D structure of hydrogel. The obtained constructs were characterized using the most relevant characterization techniques. The results showed that as-prepared nanofibers have a diameter of  $185 \pm 63$  nm and some breakages and fusions in the nanofiber's structure are apparent. The electron microscopy showed that the obtained 3D structure has a porous architecture with interconnected pores that are beneficial for bone regeneration. The biological evaluations also showed that the fabricated 3D scaffold was hemocompatible, cytocompatible, and regenerated new bone tissue in an animal model. In conclusion, these results implied that the fabricated NFC-integrated 3D scaffold exhibited promising characteristics beneficial for bone regeneration and can be applied as the bone tissue engineering scaffold.

© 2023 The Author(s). Published by Elsevier B.V. on behalf of King Saud University. This is an open access article under the CC BY-NC-ND license (<http://creativecommons.org/licenses/by-nc-nd/4.0/>).

\* Corresponding author.

E-mail addresses: [s.abbaspoor@du.ac.ir](mailto:s.abbaspoor@du.ac.ir) (S. Abbaspoor), [ah.marwan\\_bio@uoanbar.edu.iq](mailto:ah.marwan_bio@uoanbar.edu.iq) (M. Mahmood Saleh), [wangweizhuo1978@outlook.com](mailto:wangweizhuo1978@outlook.com) (W. Wang).

Peer review under responsibility of King Saud University.



## 1. Introduction

Bone serves as a mechanical support system, a binding site for muscles, ligaments, and tendons, and a shield for vital tissues, among its many other functions. The bone marrow architecture also supplies hematopoiesis and essential mineral substances. In addition to its intricate cellular structure, bone is also distinguished as a micro- and nanocomposite due to its unique organic–inorganic architecture (Benjamin et al., 2006; Kjaer, 2004; Pramanik et al., 2022). Apatite (carbonated, 65% dry weight) provides structural strength, stiffness, and mineral deposition; collagen (35% dry weight) provides rigidity, viscoelasticity, and toughness; and other proteins (non-collagenous) form a matrix/substrate stimulatory to cellular processes. Bone has the innate ability to be repaired as part of the healing period after an injury or during skeletal development, or ongoing remodeling throughout adulthood. In order to maximize skeletal repair and restore skeletal function, bone regeneration and healing is comprised of a carefully planned and organized series of biochemical and physiological reactions of bone induction and conduction involving various types of cells and cell–cell communications by some molecular–signaling pathways, with a precise temporal and spatial order (Riggs and Goodship, 2022; Henkel et al., 2013; Webster and Ahn, 2006; Vallet-Regi and Navarrete, 2016; Balasubramanian et al., 2012; Pal and Roy, 2023). The most common challenge in clinical settings is fracture repair properly, which requires mimicking the intramembranous and endochondral ossification of normal fetal skeletogenesis. Rarely do scars emerge once bony injuries (fractures) heal, and the newly created bone gradually blends in with the uninjured bone around it. This is in stark contrast to the healing process of most other tissues (Arakura et al., 2022; Dennis et al., 2015; Dimitriou et al., 2011; Nadine et al., 2022).

However, bone regeneration can be impeded in some instances of fracture healing; for instance, up to 13% of tibial fractures are linked to fracturing non-union or delayed union (Ekegren et al., 2018; Kettunen et al., 2002). Current clinical treatment options for bone fractures/defects healing, such as autologous and allogeneic transplantations using autografts and allografts, have been extensively studied, and have been reported to have significant inadequacies, limits, and consequences. In terms of bone grafts, histocompatible, non-immunogenic autografts currently represent the standard of care. While the indicated clinical intervention options have been shown to have promising effects on bone repair, none of them have all of the desired outcomes and characteristics. These include high osteoinductivity, osteoconductivity, and angiogenic potentials, biocompatibility, ready access to surgeons, a reasonable cost, and a long shelf life (Whitlock et al., 2009; Haugen et al., 2019).

TE is a promising and new method for repairing and regenerating damaged tissues. Tissue engineering has three basic principles: cell, scaffold and growth factor. The general strategy of TE is to place the cell on a scaffold designed to increase cell function and new tissue formation. Among the various scaffolds for TE applications, injectable hydrogels are similar to natural extracellular matrices due to their large amounts of water, porous structure for cell differentiation and implantation, minimally invasive implantation, simplicity of preparation and the ability to adapt well to abnormal defects, have great potential for use in TE and restorative medicine (Mistry and Mikos, 2005; Griffith and Naughton, 2002; Ikada, 2006; Ruiz-Alonso et al., 2021).

Although different natural and synthetic materials have been used to make various scaffolds, there are still limitations in various areas such as biocompatibility, cell adhesion and biodegradation rate. For tissue repair applications, such scaffolds must have mechanical, porous, and porous diameters to form new tissue. Researchers in the field of tissue engineering uses a combination of cells and polymer scaffolds to repair heart tissue in tissue engineering, there are a variety of scaffolds, including three-dimensional sponges, nanofibers and hydrogels, which will be a good choice for repairing soft tissue of hydrogel scaffolds (Thomson et al., 1995; Reddy et al., 2021; Prasad and Wong, 2018). Hydrogels are three-dimensional networks made up of hydrophilic polymers that are covalently crosslinked or held together by physical intramolecular and intermolecular interactions. Hydrogels

may absorb thousands of times their weight in water or biological fluids without disintegrating, allowing them to expand to their full size. Hydrophilicity in hydrogels is a result of the distribution of hydrophilic moieties along the polymer chain backbone, including carboxyl, amide, amino, and hydroxyl groups. Hydrogels, when inflated, have a similar soft and rubbery texture to that of biological tissues (Peppas and Hoffman, 2020; Hoffman, 2012; Mandal et al., 2020; Peppas et al., 2000).

Electrospun nanofibers have shown remarkable outcomes in bone tissue engineering approaches. Materials with their unique biocompatibility, mechanical strength, and biodegradability can be electrospun into nanofibers (Fadil et al., 2021; Zhang et al., 2020). Blended electrospinning, multi-axial electrospinning, coaxial electrospinning, and so on are only a few examples of the spinning methods that can be used to prepare electrospun nanofibers with a wide range of possible topologies (Luraghi et al., 2021; Huang et al., 2022). However, when used in BTE, the electrospun scaffolds cannot show their highest healing performance due to their 2D structure. For this reason, electrospun nanofibers have been subjected to a wide range of modifications in an effort to enhance their capabilities for stimulating bone formation. Their combination with 3D scaffolds, such as hydrogels, is an alternative option (Zhang et al., 2008; Jang et al., 2009; Wang et al., 2018; Ye et al., 2019; Wang et al., 2010). In the current assay, we fabricated electrospun nanofibrous carbon and combined them with alginate CMC hydrogel.

## 2. Experimental details

### 2.1. Materials

The sources of supply of chemicals and reagents used in this study are as follows: Merck (Darmstadt, Germany) provided Polyacrylonitrile (PAN, average Mw 150,000), Sodium alginate (MW: 12 k, Pharmaceutical grade), DMF, CaCl<sub>2</sub> (>97%), and DMSO. Gibco, BRL (Eggenstein, Germany) provided Pen/Strep, MTT assay kit, DMEM/F12, and FBS.

### 2.2. Nanofibers manufacture

According to the previously established protocol, in a two-stage heat treatment, Electrospun NFCs were extracted from PAN nanofibers. By dissolving a certain amount of PAN polymer in DMF and setting the concentration at 10% wt % and stirring suspension regularly at 37 °C for 24 h until obtaining a clear and homogeneous polymer solution PAN nanofibers were produced. Using the electrospinning device and adjusting the feed rate of one milliliter per minute, the voltage of 18 kV and the distance from the needle to the collector equal to 12 cm of the provided PAN/DMF solution was electrospun. The mat made of PAN nanofiber was then peeled off and after being collected from the collector, for heating treatment, it was placed in a furnace. The performed heat treatments for NFC fabrication involved the stabilization process (1.0 °C/min up to 250 °C and stabilized at this temperature 2 h) and carbonization (5 °C/min up to 1000 °C and carbonization at this temperature for 1 h under Ar gas) (Abd El-Aziz et al., 2017; Chen et al., 2010; Rahaman et al., 2007).

### 2.3. Hydrogel synthesis

The hydrogel nanocomposites were synthesized based on the physical cross-linking of alginate polymer using CaCl<sub>2</sub>. NFC were crashed and added to deionized (DI) water to obtain

three different concentrations (1, 5, and 10 wt%, respect to the dry weight of alginate), stirred for 24 h, and sonicated several times to completely disperse the NFC. Then, specific amount of alginate was added to the as-prepared NFC/DI water solution with the final concentration if 2 wt% and stirred for 12 h to completely dissolve the polymer. Finally, CaCl<sub>2</sub> solution (100 mM) was added to the Alg/NFC solution and gently mixed to initiate the physical cross-linking. The fabricated hydrogel nanocomposites were lyophilized for further characterization and applications. The samples were frozen for 12 h at  $-20^{\circ}\text{C}$ , then freeze-dried using a freeze drier (Telstar, Terrassa, Spain) for 24 h at  $-80^{\circ}\text{C}$ .

#### 2.4. Hydrogel characterization

The internal morphology and pores arrangement of the obtained hydrogel nanocomposites were evaluated using SEM imaging technique after sputter-coating with a thin layer of gold (Kim and Chu, 2000; Podhorská et al., 2020). The pore diameter of the samples was measured according to the obtained SEM micrographs using ImageJ software (NIH, Bethesda, USA).

The porosity (%) of as-prepared hydrogel samples was measured according to the liquid displacement method (Qin et al., 2018; Wang et al., 2017). Briefly, a specific among of the hydrogel nanocomposites was soaked in absolute ethanol for 1 h and then remove. The primary volume of solution ( $V_1$ ), the volume changes after soaking ( $V_2$ ) and removing hydrogels ( $V_3$ ) were used to calculate the porosity based on Eq. (1).

$$\text{Porosity (\%)} = \left( \frac{V_1 - V_3}{V_2 - V_3} \right) \times 100 \quad (1)$$

The water absorption and retention of as-prepared hydrogel samples were assessed based on the gravimetric and weighing method (Arpornmaeklong et al., 2021; Shen et al., 2013). As-prepared hydrogel samples were weighed and submerged into PBS (pH: 7.4) at room temperature for 72 h. At the pre-determined time points, the scaffolds were removed and weighed again. The swelling kinetics of as-prepared hydrogel samples was calculated using Eq. (2).

$$\text{Mass swelling (\%)} = \left( \frac{W_1 - W_0}{W_0} \right) \times 100 \quad (2)$$

$W_0$ : dry sample and  $W_1$ : swelled sample

#### 2.5. In vitro studies

##### 2.5.1. Hemocompatibility

Hemocompatibility of as-prepared hydrogel samples was assessed based on the measuring the induced hemolysis (Eivazzadeh-Keihan et al., 2022). 0.2 mL of fresh blood containing anticoagulant agent (EDTA) was incubated with 50 mg of the hydrogels at  $37^{\circ}\text{C}$  for 1 h. Then, the blood incubated with samples was centrifuged (1500 rpm,  $4^{\circ}\text{C}$ ) and a Microplate reader was applied to read the absorbance of the supernatant at 545 nm. The hemolysis percent was calculated using Eq. (3).

$$\text{Hemolysis (\%)} = \left( \frac{Dt - Dnc}{Dpc - Dnc} \right) \times 100 \quad (3)$$

Where  $Dt$ ,  $Dnc$ , and  $Dpc$  were absorbance of the sample, absorbance of the NC and absorbance of the PC.

##### 2.5.2. Cell viability/proliferation

The viability of bone cells (MG-63 cells) on/into the as-prepared hydrogel samples was measured using the MTT assay technique. As-prepared samples were sterilized using ETOH (70%) for 2 h following several washes with sterilized PBS. A number of  $1 \times 10^4$  cells were suspended in 0.1 mL cell culture medium bearing FBS (10 %v/v) and antibiotics were incubated with the samples at  $37^{\circ}\text{C}$  with 5% CO<sub>2</sub> in a humidified incubator for two and three days. After passing the time points, the medium was removed and replaced with the MTT salt.

#### 2.6. In vivo studies

For animal study and bone defect induction experiments, ten adult male Wistar rats served as the subjects. The protocols for the animal experiments and assessments were developed using the ARRIVE guidelines (<https://arriveguidelines.org>) and according to the related guidelines. The animals were put to sleep by intraperitoneal (IP) injection of a xylazine:ketamine mixture. Using the trephine, we generated a 6 mm segmental damage in the rat bone. Five rats each were assigned to the control (defect, no treatment) and scaffold treatment groups. After the periosteum was reattached, 30 mg of as-prepared scaffolds were implanted into the defect site. The proper sutures were used to close the muscle and skin layers. Tissues were taken 2 months after surgery and fixed in 10% neutral buffered formalin for 48 h before the animals were slaughtered. Bone samples were decalcified in 5% nitric acid for 10 days. Finally, 5  $\mu\text{m}$  thick slices were cut and stained with H&E staining and Masson's trichrome from the decalcified samples (MT). The independent pathologist used light microscopy to analyze the histology slides. Both the amount of surviving implants and the amount of newly produced cartilage or bone were measured in relation to the entire area of the section. Cells were counted using a magnification of 400 using the computer software Image-Pro Plus® V.6 for histomorphometric analysis.

#### 2.7. Statistical analysis

Mean and standard deviation were used to describe and two-sample independent *t*-test and one-way analysis of variance were used for analysis. Bonferroni test was used for pairwise comparisons after analysis of variance. All analyzes were performed in SPSS 19 software. Significance level in all tests was considered 5%.

### 3. Results and discussion

#### 3.1. Nanofibers morphology

Nanofibers are sophisticated nanomaterials with remarkable properties. Nanofibers are a promising new fibrous material with potential applications in polymer matrix reinforcement and modification. The unique characteristics of nanofibers have garnered a lot of attention. Nanofibers are appropriate

for a wide variety of applications, including filtration, sensing, bioengineering, functional materials, and energy storage, since they are lightweight, have small diameters, have customizable pore architectures, and have a high surface-to-volume ratio. But the potential of new composite nanofibers is much higher, and research into novel polymer composite nanofibers has sparked widespread attention as a means of expanding their multifunctional potential and improving their chemical and physical properties. Composite nanofibers made of polymers can include anything from polymer/polymer nanofibers to polymer/nanoparticle composite nanofibers to polymer/inorganic salts composite nanofibers (Yoon et al., 2008; Lou et al., 2020; Wang et al., 2009; Cho et al., 2012). SEM imaging was conducted to evaluate the morphology of as-prepared NFC and the results are presented in Fig. 1. The results showed that as-prepared nanofibers have a diameter of  $185 \pm 63$  nm and some breakages and fusions in NFC structure are apparent. These breakages and fusions in NFC structure could be induced during the heat treatment and carbonization process.

### 3.2. Hydrogel characteristics

Microarchitecture, in biology, is the microscopic architecture of any organ. The sol–gel transition organization of the polymer network, polymer concentration, and cross-linking parameters (e.g., ionic strength, temperature, and pH) all have a role in determining the hydrogel’s microarchitecture. Mesh size, also known as molecular porosity, is a measure of the resulting polymer network’s ability to allow gas exchange and nutrient uptake (Laronda et al., 2017; Park et al., 2002; Caliarì and Burdick, 2016). Fig. 2 shows micrographs of hydrogel scaffolds, which reveal that the scaffolds have a porous structure with pores that are connected to one another. The pores range in dimensions and are not all aligned in the same way. Furthermore, there were no signs of phase separation, demonstrating the high compatibility of the scaffold synthesis components.

A homogeneous porous structure with interconnecting open pores of circular and irregular geometries characterizes the Alg/CMC scaffold, reflecting its internal morphology. Scaffolds made from alginate and carboxymethyl cellulose (CMC) are polymeric structures that can efficiently distribute

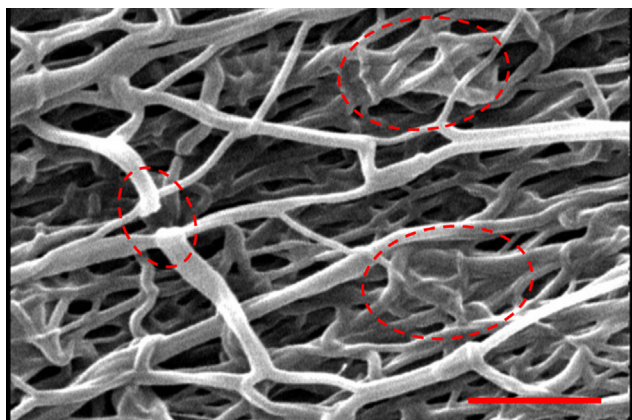


Fig. 1 SEM image of the nanofibers. Scale bar: 2  $\mu$ m.

nutrients, which is required for cellular vascularization, proliferation, and differentiation. In a similar vein, micrographs of the Alg/CMC scaffold’s surface revealed the various pore sizes and interconnections present, indicating that the detected surface porosity can improve the relationships between these biomaterials designed for tissue regeneration and cells, implying their faster attachment.

Bone ingrowth is primarily influenced by porosity, pore size, pore shape, and pore distribution at random. Cells are given enough room to multiply thanks to the porous structure’s sufficient area. Permeability can be affected by pore shape, which in turn affects bone ingrowth. The bone’s interior structure is reflected in the porous structure found throughout (Poh et al., 2019). Even though recently developed randomized structures like Voronoi can successfully mimic the structure of bone, discussion on the nature of randomization is rarely engaged. The long-term bone healing response is greatly influenced by the early stress stimulus. Scaffolds with Young’s modulus close to that of bone can effectively mitigate the stress-shielding effect. Various studies have demonstrated that Young’s modulus and compressive strength are inversely related. Modifying the porosity and pore shape can restore harmony to the connection between them. On the other hand, with maximum load, different pore shapes fail in different directions. So, similar to bone, orthopedic scaffolds need to have a suitable pore size and porosity, a reasonable pore shape, and a random or gradient pore distribution (Chen et al., 2020).

According to Table 1 and Fig. 3, the results of the one-way analysis of variance test showed that the mean porosity score was significantly different in all groups ( $p = 0.002$ ). Then Bonferroni test was performed to compare two by two groups and the results showed that only Alg/CMC with Alg/CMC/NFC 10% and group Alg/CMC with Alg/CMC/NFC 5% had significant differences, which are also shown in Fig. 3.

In the field of tissue engineering, the swelling capacity of the scaffolds is a crucial performance indicator. Pore size, connectivity conditions, and scaffold volume are all involved. The ability to swell plays a crucial role in the uptake of bodily fluid and the transport of cellular nutrients and metabolites. Swelling helps cells invade scaffolds in a three-dimensional pattern during cell culture. The total porosity and pore size both increase during swelling, making the most of the scaffolds’ internal surface area. Samples with a greater degree of swelling will have a bigger surface area/volume ratio, increasing the likelihood of cell infusion into the three-dimensional scaffold and fostering greater cell development through improved adhesion to the scaffold surface. The enhanced availability of the samples for nutrients from the culture media is another benefit of the excessive swelling. Though scaffold swelling would benefit cell adherence, it might have a negative impact on the scaffolds’ mechanical qualities. The results of the swelling measurement (Fig. 4) show that as-prepared constructs swelled in PBS solution.

### 3.3. Hemocompatibility results

The scaffolds’ high sensitivity to hemolysis when exposed to blood is a major drawback to using them as bone transplant alternatives. Blood cell membranes are broken or erythrocytes are lysed, releasing their intracellular hemoglobin, as a result

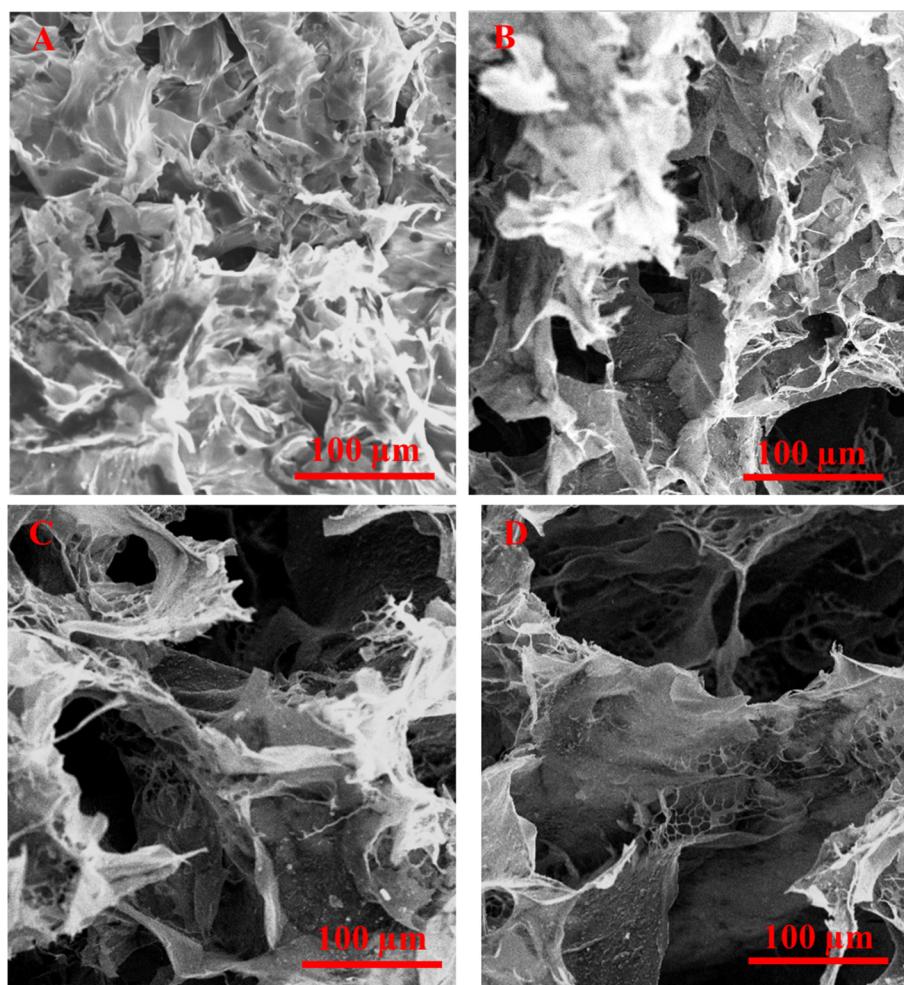


**Fig. 2** SEM micrograph of (A) Alg/CMC, (B) Alg/CMC/NFC 1%, (C) Alg/CMC/NFC 5%, and (D) Alg/CMC/NFC 10%.

**Table 1** Results of comparing Porosity score.

Hydrogel synthesis	Porosity Score			Mean	SD	P value
	S 1	S 2	S 3			
Alg/CMC	70	67	73	70	3	0.002
Alg/CMC/NFC 1%	75	78	73	75.3	2.51	
Alg/CMC/NFC 5%	82	85	79	82	3	
Alg/CMC/NFC 10%	85	88	80	84.3	4.04	

Alg: Alginate.

CMC: Carboxymethyl cellulose (CMC).

NFC: Nanofibrous carbon.

of the contact. In order to prevent the implanted substance from being harmful, the amount of hemoglobin discharged should be low. Additionally, the hemocompatibility of biomaterials in direct interaction with bone tissue may have an effect on osseointegration. Given that blood will be the predominant fluid in touch with implants, their hemocompatibility has been considered in terms of hemolysis, or the breakdown of RBCs after substrate interaction, blood cell adhesion on the surface of biomaterial, and platelet adhesion. Blood clots accumulate and stabilize damaged bone tissue during the healing process, while the dissolution of hematoma offers the components that

initiate chemotaxis for cell-mediated repair of the bone tissue (Chi Perera et al., 2020; Padalhin et al., 2014; Alehosseini et al., 2018).

As can be seen in Table 2, the results of the one-way analysis of the variance test showed that the mean Hemocompatibility score was not significantly different in all groups (without the control group) ( $p = 0.11$ ). Considering the information of the control group and performing the one-way analysis of variance test, the test result shows a significant difference significant differences are related to the comparison of all groups with the control group ( $p = 0.004$ ).

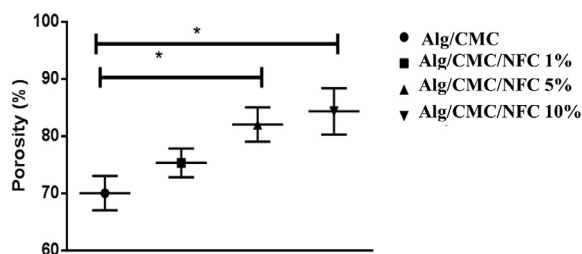


**Fig. 3** Porosity percentage of the prepared hydrogel nanocomposites: \*significant difference.

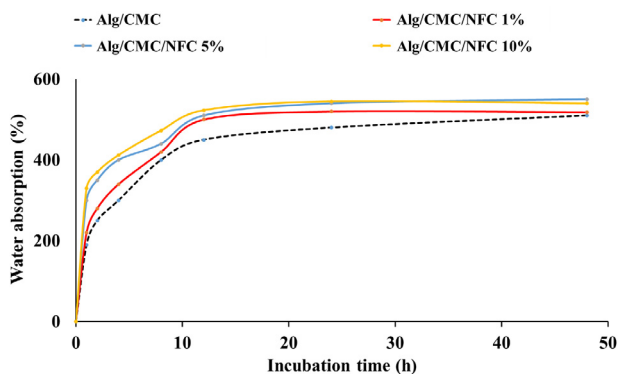


**Fig. 4** Water absorption of the prepared hydrogel nanocomposites.

### 3.4. Cell culture finding

Cytocompatibility is a critical property for bone TE scaffolds and determines the fate of the applied treatment strategy. The cell culture study using bone cells (MG-63 cell line) was conducted to reveal the biocompatibility and cytocompatibility of as-prepared scaffolds.

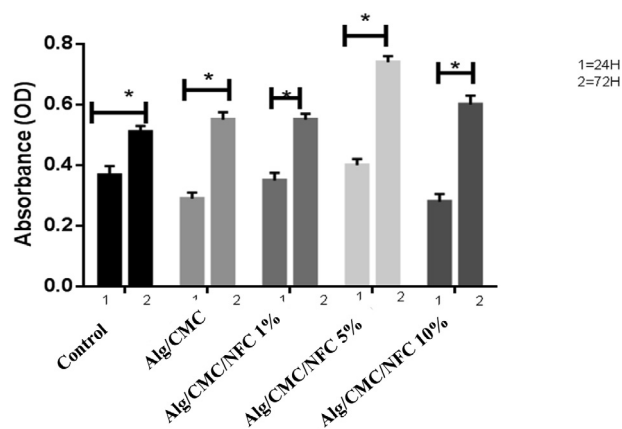


**Fig. 5** Viability of MG-63 cells on the prepared hydrogel nanocomposites measured by the MTT assay kit. Values represent the mean  $\pm$  SD, n: 5, \*  $p < 0.05$ , (obtained by one-way ANOVA).

According to [Table 3](#), and [Fig. 5](#) the results of two independent samples *t*-test showed that in each group, the 72-hour profiling score is significantly higher compared to the 24-hour one. These differences are also shown in [Fig. 5](#).

### 3.5. In vivo bone healing results

All the samples were visualized by an independent reviewer 60 days after the implanting procedure. The results of the histomorphometric analysis were obtained based on the histopathological observations ([Fig. 6](#)) and the histopathological evaluation and have been reported in [Table 4](#). Micrograph of samples showed a massive fibrocartilaginous tissue formation, following newly formed bone tissue. Histopathological evaluation of this sample revealed appropriate neovascularization along with new bone formation. Histomorphometric analysis of samples showed a massive fibrocartilaginous tissue

**Table 2** Results of comparing Hemocompatibility.

	S 1	S 2	S 3	Mean	SD	p value	all groups comparing- p value
Control	100	100	100	100	0		0.004
Alg/CMC	6	4	7	5.66	1.52	0.11	
Alg/CMC/NFC 1%	7	9	6	7.33	1.52		
Alg/CMC/NFC 5%	6	7	4	5.66	1.52		
Alg/CMC/NFC 10%	9	7	11	9	2		

**Table 3** Results of comparing Cell proliferation.

Group	Time			Mean (SD)	72H	P	Mean (SD)	P	
	24H								
Control	0.31	0.29	0.35	0.32(0.03)	0.5	0.53	0.49	0.51(0.02)	< 0.001
Alg/CMC	0.29	0.31	0.27	0.29(0.02)	0.55	0.57	0.52	0.55(0.02)	< 0.001
Alg/CMC/NFC 1%	0.35	0.32	0.37	0.35(0.02)	0.65	0.68	0.32	0.55(0.2)	< 0.001
Alg/CMC/NFC 5%	0.4	0.42	0.38	0.4 (0.02)	0.75	0.72	0.76	0.74(0.02)	< 0.001
Alg/CMC/NFC 10%	0.28	0.25	0.3	0.27(0.02)	0.6	0.57	0.63	0.6(0.03)	< 0.001

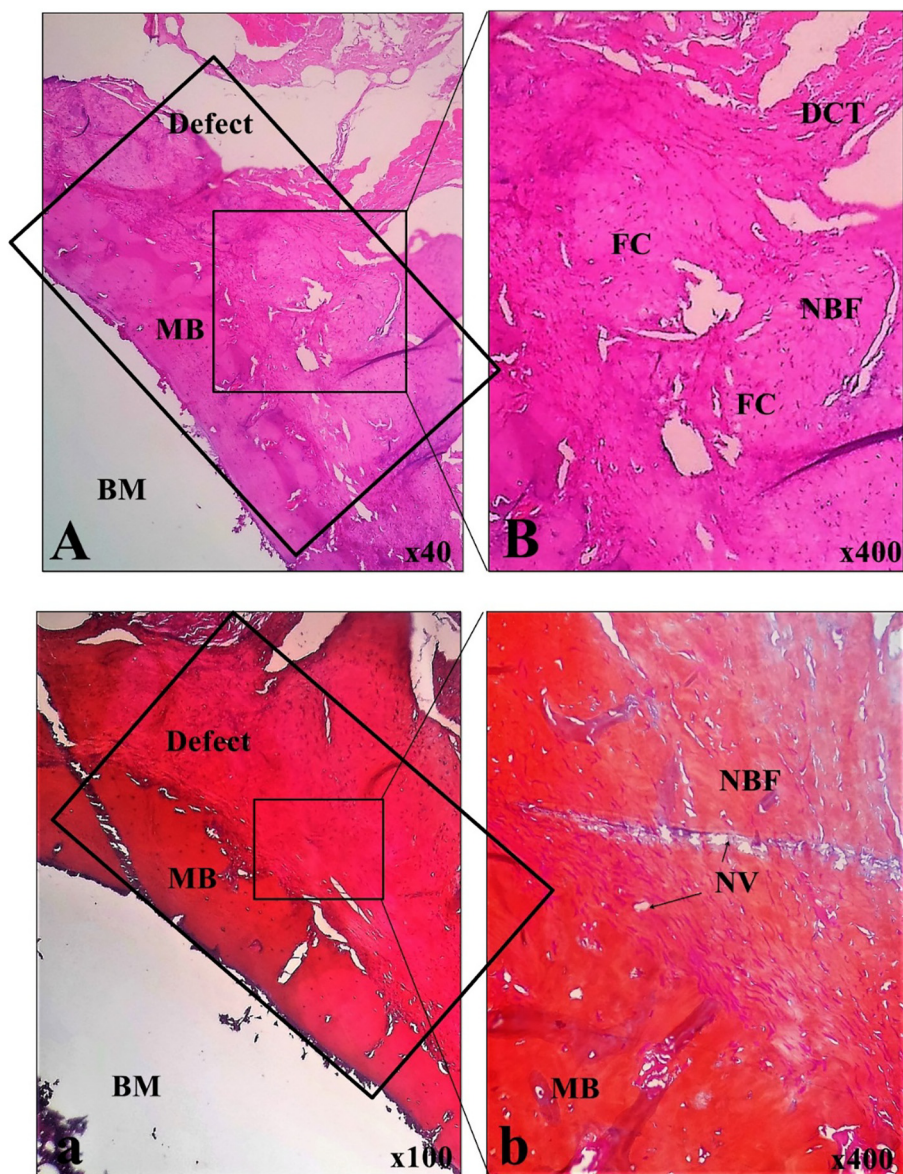


**Fig. 6** Histopathological findings of implanted materials in the experimental femoral defect. BM: bone marrow, NBF: new bone formation, MB: mature bone, DCT: dense connective tissue, NV: neovascularization, FC: fibrocartilage; A and B: H&E stain, a and b: MT stain.

**Table 4** Histomorphometric results.

Valuable	Scaffold
Fibroblast + fibrocyte	112.23 ± 12.08
Chondroblast + chondrocyte	21.10 ± 5.22
Osteoblast + osteocyte	24.33 ± 1.07
Osteoclast	00.00
Osteon	0.91 ± 0.07
NBF (%)	31.86 ± 6.45

formation, following newly formed bone tissue. Histopathological evaluation of this sample revealed an appropriate neovascularization along with new bone formation.

#### 4. Conclusion

Tissue engineering is a relatively new subject, yet advancements have been modest despite its nearly two decade history. An ideal scaffold must satisfy both physical and biological criteria, and this requires a delicate balancing act between the complexity of material designs that include pore gradients and different material combinations and the sophistication of nanoscale functional capabilities achieved through surface modification, cell entrapment, and controlled chemical release. Because of their capacity to imitate the original structure of the ECM, enhance cell adhesion, and induce cell differentiation, nanofibrous electrospun mats have found extensive utility in tissue engineering. Yet nanofibers' small pores aren't big enough to let cells move into the scaffold or nutrients diffuse through them. To this end, we sought to create a scaffold that most closely resembled natural bone by fusing the 3D scaffold idea (the hydrogel) with nanofibers (NFC). In the light of this, we combined the NFC as the filler to 3D hydrogel scaffolds fabricated from alginate and CMC.

The results clearly indicated that the fabricated scaffolds have acceptable physical, structural, and biological properties suitable for bone tissue engineering and regeneration. Our findings revealed that Alg/CMC/NFC 5% exhibited best biological performance and induced the highest cell proliferation. The animal studies using this scaffold (Alg/CMC/NFC 5%) revealed that at the optimum condition, the developed structure can promote bone regeneration and fill the bone defect. These results indicate that the fabricated scaffolds can be applied as the bone tissue engineering construct.

### Ethical Compliance

Research experiments conducted in this article with animals were approved by the Ethical Committee and responsible authorities of our research organization(s) following all guidelines, regulations, legal, and ethical standards as required for animals.

### Conflicts of Interest

The authors declare no conflicts of interest

### Acknowledgments

Natural Science Foundation of China, Grant/Award Number: No.81001225

International Co-operative Plan of Shaanxi, Grant/Award Number: S2016YFKW0013.

### References

- Abd El-Aziz, A., El Backly, R.M., Taha, N.A., El-Maghraby, A., Kandil, S.H., 2017. Preparation and characterization of carbon nanofibrous/hydroxyapatite sheets for bone tissue engineering. *Materials Science and Engineering: C*. 76, 1188–1195.
- Alehosseini, M., Golafshan, N., Kharaziha, M., Fathi, M., Edris, H., 2018. Hemocompatible and bioactive heparin-loaded PCL- $\alpha$ -TCP fibrous membranes for bone tissue engineering. *Macromolecular Bioscience*. 18, 1800020.
- Arakura, M., Lee, S.Y., Fukui, T., Oe, K., Takahara, S., Matsumoto, T., Hayashi, S., Matsushita, T., Kuroda, R., Niikura, T., 2022. Endochondral bone tissue engineering using human induced pluripotent stem cells. *Tissue Engineering Part A*. 28, 184–195.
- Arpornmaeklong, P., Sareethammanuwat, M., Apinyaupatham, K., Boonyuen, S., 2021. Characteristics and biologic effects of thermosensitive quercetin-chitosan/collagen hydrogel on human periodontal ligament stem cells. *Journal of Biomedical Materials Research Part B: Applied Biomaterials*. 109, 1656–1670.
- Balasubramanian, P., Prabhakaran, M.P., Sireesha, M., Ramakrishna, S., 2012. Collagen in human tissues: structure, function, and biomedical implications from a tissue engineering perspective. *Polymer Composites-Polyolefin Fractionation-Polymeric Peptidomimetics-Collagens*, 173–206
- Benjamin, M., Toumi, H., Ralphs, J.R., Bydder, G., Best, T., Milz, S., 2006. Where tendons and ligaments meet bone: attachment sites ("entheses") in relation to exercise and/or mechanical load. *Journal of anatomy*. 208, 471–490.
- Caliari, S.R., Burdick, J.A., 2016. A practical guide to hydrogels for cell culture. *Nature methods*. 13, 405–414.
- Chen, H., Han, Q., Wang, C., Liu, Y., Chen, B., Wang, J., 2020. Porous scaffold design for additive manufacturing in orthopedics: A review. *Frontiers in Bioengineering and Biotechnology*. 8, 609.
- Chen, I.-H., Wang, C.-C., Chen, C.-Y., 2010. Fabrication and characterization of magnetic cobalt ferrite/polyacrylonitrile and cobalt ferrite/carbon nanofibers by electrospinning. *Carbon*. 48, 604–611.
- Chi Perera, C.J., Castillo Baas, M.G., Alcocer Lara, G.A., Ramos Borges, S.I., Rodríguez Guzmán, A.L., Fernández Cervantes, I., Rodríguez Fuentes, N., 2020. Characterization and hemocompatibility assessment of porous composite scaffolds with a biomimetic human clavicle macrostructure. *Health and Technology*. 10, 423–428.
- Cho, D., Lee, S., Frey, M.W., 2012. Characterizing zeta potential of functional nanofibers in a microfluidic device. *Journal of colloid and interface science*. 372, 252–260.
- Dennis, S.C., Berkland, C.J., Bonewald, L.F., Detamore, M.S., 2015. Endochondral ossification for enhancing bone regeneration: converging native extracellular matrix biomaterials and developmental engineering in vivo. *Tissue Engineering Part B: Reviews*. 21, 247–266.
- Dimitriou, R., Jones, E., McGonagle, D., Giannoudis, P.V., 2011. Bone regeneration: current concepts and future directions. *BMC medicine*. 9, 1–10.
- Eivazzadeh-Keihan, R., Choopani, L., Aliabadi, H.A.M., Ganjali, F., Kashtiaray, A., Maleki, A., Cohan, R.A., Bani, M.S., Komijani, S., Ahadian, M.M., 2022. Magnetic carboxymethyl cellulose/silk fibroin hydrogel embedded with halloysite nanotubes as a biocompatible nanobiocomposite with hyperthermia application. *Materials Chemistry and Physics*. 287, 126347.
- Ekegren, C.L., Edwards, E.R., De Steiger, R., Gabbe, B.J., 2018. Incidence, costs and predictors of non-union, delayed union and mal-union following long bone fracture. *International Journal of Environmental Research and Public Health*. 15, 2845.
- Fadil, F., Affandi, N.D.N., Misnon, M.I., Bonnia, N.N., Harun, A. M., Alam, M.K., 2021. Review on electrospun nanofiber-applied products. *Polymers*. 13, 2087.
- Griffith, L.G., Naughton, G., 2002. Tissue engineering—current challenges and expanding opportunities. *science*. 295, 1009–1014.
- Haugen, H.J., Lyngstadaas, S.P., Rossi, F., Perale, G., 2019. Bone grafts: which is the ideal biomaterial? *Journal of Clinical Periodontology*. 46, 92–102.
- Henkel, J., Woodruff, M.A., Epari, D.R., Steck, R., Glatt, V., Dickinson, I.C., Choong, P.F., Schuetz, M.A., Hutmacher, D.W., 2013. Bone regeneration based on tissue engineering conceptions—a 21st century perspective. *Bone research*. 1, 216–248.
- Hoffman, A.S., 2012. Hydrogels for biomedical applications. *Advanced drug delivery reviews*. 64, 18–23.
- Huang, C., Xu, X., Fu, J., Yu, D.-G., Liu, Y., 2022. Recent progress in electrospun polyacrylonitrile nanofiber-based wound dressing. *Polymers*. 14, 3266.
- Ikada, Y., 2006. Challenges in tissue engineering. *Journal of the Royal Society Interface*. 3, 589–601.
- Jang, J.-H., Castano, O., Kim, H.-W., 2009. Electrospun materials as potential platforms for bone tissue engineering. *Advanced drug delivery reviews*. 61, 1065–1083.
- Kettunen, J., Mäkelä, E., Turunen, V., Suomalainen, O., Partanen, K., 2002. Percutaneous bone grafting in the treatment of the delayed union and non-union of tibial fractures. *Injury*. 33, 239–245.
- Kim, S.H., Chu, C.C., 2000. Pore structure analysis of swollen dextran-methacrylate hydrogels by SEM and mercury intrusion porosimetry. *Journal of Biomedical Materials Research: An Official Journal of The Society for Biomaterials, The Japanese Society for Biomaterials, and The Australian Society for Biomaterials and the Korean Society for Biomaterials*. 53, 258–266.
- Kjaer, M., 2004. Role of extracellular matrix in adaptation of tendon and skeletal muscle to mechanical loading. *Physiological reviews*. 84, 649–698.
- Laronda, M.M., Rutz, A.L., Xiao, S., Whelan, K.A., Duncan, F.E., Roth, E.W., Woodruff, T.K., Shah, R.N., 2017. A bioprosthetic ovary created using 3D printed microporous scaffolds restores ovarian function in sterilized mice. *Nature communications*. 8, 1–10.

- Lou, L., Osemwegie, O., Ramkumar, S.S., 2020. Functional nanofibers and their applications. *Industrial & Engineering Chemistry Research*. 59, 5439–5455.
- Luraghi, A., Peri, F., Moroni, L., 2021. Electrospinning for drug delivery applications: A review. *Journal of Controlled release*. 334, 463–484.
- Mandal, A., Clegg, J.R., Anselmo, A.C., Mitragotri, S., 2020. Hydrogels in the clinic. *Bioengineering & translational medicine*. 5, e10158.
- Mistry, A.S., Mikos, A.G., 2005. Tissue engineering strategies for bone regeneration. *Regenerative medicine II*. 1–22.
- Nadine, S., Fernandes, I.J., Correia, C.R., Mano, J.F., 2022. Close-to-native bone repair via tissue engineered endochondral ossification approaches. *Iscience*. 105370.
- Padalhin, A.R., Thuy Ba Linh, N., Ki Min, Y., Lee, B.-T., 2014. Evaluation of the cytocompatibility hemocompatibility in vivo bone tissue regenerating capability of different PCL blends. *Journal of Biomaterials Science, Polymer Edition*. 25, 487–503.
- Pal, V.K., Roy, S., 2023. Cooperative Calcium Phosphate Deposition on Collagen-Inspired Short Peptide Nanofibers for Application in Bone Tissue Engineering. *Biomacromolecules*.
- Park, S.-N., Park, J.-C., Kim, H.O., Song, M.J., Suh, H., 2002. Characterization of porous collagen/hyaluronic acid scaffold modified by 1-ethyl-3-(3-dimethylaminopropyl) carbodiimide cross-linking. *Biomaterials*. 23, 1205–1212.
- Peppas, N.A., Bures, P., Leobandung, W., Ichikawa, H., 2000. Hydrogels in pharmaceutical formulations. *European journal of pharmaceutics and biopharmaceutics*. 50, 27–46.
- Peppas, N.A., Hoffman, A.S., 2020. In Biomaterials science. Elsevier.
- Podhorská, B., Vetrík, M., Chylíková-Krumbholcová, E., Kománková, L., Rashedí Banafshehvaragh, N., Šlouf, M., Dušková-Smrčková, M., Janoušková, O., 2020. Revealing the true morphological structure of macroporous soft hydrogels for tissue engineering. *Applied Sciences*. 10, 6672.
- Poh, P.S., Valainis, D., Bhattacharya, K., Van Griensven, M., Dondl, P., 2019. Optimization of bone scaffold porosity distributions. *Scientific reports*. 9, 1–10.
- Pramanik, S., Kharche, S., More, N., Ranglani, D., Kapusetti, G., 2022. Natural Biopolymers for Bone Tissue Engineering. A Brief Review, *Engineered Regeneration*.
- Prasadh, S., Wong, R.C.W., 2018. Unraveling the mechanical strength of biomaterials used as a bone scaffold in oral and maxillofacial defects. *Oral Science International*. 15, 48–55.
- Qin, H., Wang, J., Wang, T., Gao, X., Wan, Q., Pei, X., 2018. Preparation and characterization of chitosan/ $\beta$ -glycerophosphate thermal-sensitive hydrogel reinforced by graphene oxide. *Frontiers in chemistry*. 6, 565.
- Rahaman, M.S.A., Ismail, A.F., Mustafa, A., 2007. A review of heat treatment on polyacrylonitrile fiber. *Polymer degradation and Stability*. 92, 1421–1432.
- Reddy, M.S.B., Ponnamma, D., Choudhary, R., Sadasivuni, K.K., 2021. A comparative review of natural and synthetic biopolymer composite scaffolds. *Polymers*. 13, 1105.
- Riggs, C., Goodship, A., 2022. Bone Structure and Function. *Fractures in the Horse*. 11–27.
- Ruiz-Alonso, S., Lafuente-Merchan, M., Ciriza, J., Saenz-del-Burgo, L., Pedraz, J.L., 2021. Tendon tissue engineering: Cells, growth factors, scaffolds and production techniques. *Journal of Controlled Release*. 333, 448–486.
- Shen, S., Fu, D., Xu, F., Long, T., Hong, F., Wang, J., 2013. The design and features of apatite-coated chitosan microspheres as injectable scaffold for bone tissue engineering. *Biomedical Materials*. 8, 025007.
- Thomson, R., Wake, M., Yaszemski, M., Mikos, A., 1995. In *Biopolymers II*. Springer.
- Vallet-Regi, M., and Navarrete, D. A. 2016. *Biological apatites in bone and teeth, Nanoceramics in Clinical Use: From Materials to Applications*, Vallet-Regi, M., Arcos Navarrete, D., (Eds.), 2nd ed. 1-29.
- Wang, Y., Cui, W., Chou, J., Wen, S., Sun, Y., Zhang, H., 2018. Electrospun nanosilicates-based organic/inorganic nanofibers for potential bone tissue engineering. *Colloids and Surfaces B: Biointerfaces*. 172, 90–97.
- Wang, H.-S., Fu, G.-D., Li, X.-S., 2009. Functional polymeric nanofibers from electrospinning. *Recent patents on nanotechnology*. 3, 21–31.
- Wang, J., Valmikinathan, C.M., Liu, W., Laurencin, C.T., Yu, X., 2010. Spiral-structured, nanofibrous, 3D scaffolds for bone tissue engineering. *Journal of Biomedical Materials Research Part A: An Official Journal of The Society for Biomaterials. The Japanese Society for Biomaterials, and The Australian Society for Biomaterials and the Korean Society for Biomaterials*. 93, 753–762.
- Wang, J., Hao, S., Luo, T., Cheng, Z., Li, W., Gao, F., Guo, T., Gong, Y., Wang, B., 2017. Feather keratin hydrogel for wound repair: preparation, healing effect and biocompatibility evaluation. *Colloids and Surfaces B: Biointerfaces*. 149, 341–350.
- Webster, T.J., Ahn, E.S., 2006. Nanostructured biomaterials for tissue engineering bone. *Tissue Engineering II*. 275–308.
- Whitlock, E.L., Tuffaha, S.H., Luciano, J.P., Yan, Y., Hunter, D.A., Magill, C.K., Moore, A.M., Tong, A.Y., Mackinnon, S.E., Borschel, G.H., 2009. Processed allografts and type I collagen conduits for repair of peripheral nerve gaps. *Muscle & Nerve: Official Journal of the American Association of Electrodiagnostic Medicine*. 39, 787–799.
- Ye, K., Kuang, H., You, Z., Morsi, Y., Mo, X., 2019. Electrospun nanofibers for tissue engineering with drug loading and release. *Pharmaceutics*. 11, 182.
- Yoon, K., Hsiao, B.S., Chu, B., 2008. Functional nanofibers for environmental applications. *Journal of Materials Chemistry*. 18, 5326–5334.
- Zhang, W., He, Z., Han, Y., Jiang, Q., Zhan, C., Zhang, K., Li, Z., Zhang, R., 2020. Structural design and environmental applications of electrospun nanofibers. *Composites Part A: Applied Science and Manufacturing*. 137, 106009.
- Zhang, Y., Venugopal, J.R., El-Turki, A., Ramakrishna, S., Su, B., Lim, C.T., 2008. Electrospun biomimetic nanocomposite nanofibers of hydroxyapatite/chitosan for bone tissue engineering. *Biomaterials*. 29, 4314–4322.